

Video Article

Kinematic History of a Salient-recess Junction Explored through a Combined Approach of Field Data and Analog Sandbox Modeling

Zeshan Ismat^{*1}, Kevin Toeneboehn^{*2}

¹Department of Earth and Environmental Science, Franklin and Marshall College

²Department of Geosciences, University of Massachusetts, Amherst

*These authors contributed equally

Correspondence to: Zeshan Ismat at zeshan.ismat@fandm.edu

URL: <https://www.jove.com/video/54318>

DOI: [doi:10.3791/54318](https://doi.org/10.3791/54318)

Keywords: Environmental Sciences, Issue 114, fold-thrust belt, Sevier, oblique ramp, faults, sandbox models, cataclastic flow

Date Published: 8/5/2016

Citation: Ismat, Z., Toeneboehn, K. Kinematic History of a Salient-recess Junction Explored through a Combined Approach of Field Data and Analog Sandbox Modeling. *J. Vis. Exp.* (114), e54318, doi:10.3791/54318 (2016).

Abstract

Within fold-thrust belts, the junctions between salients and recesses may hold critical clues to the overall kinematic history. The deformation history within these junctions is best preserved in areas where thrust sheets extend from a salient through an adjacent recess. We examine one such junction within the Sevier fold-thrust belt (western United States) along the Leamington transverse zone, northern Utah. Deformation within this junction took place by faulting and cataclastic flow. Here, we describe a protocol that examines these fault patterns to better understand the kinematic history of the field area. Fault data is supplemented by analog sandbox experiments. This study suggests that, in detail, deformation within the overlying thrust sheet may not directly reflect the underlying basement structure. We demonstrate that this combined field-experimental approach is easy, accessible, and may provide more details to the deformation preserved in the crust than other more expensive methods, such as computer modeling. In addition, the sandbox model may help to explain why and how these details formed. This method can be applied throughout fold-thrust belts, where upper-crustal rocks are well preserved. In addition, it can be modified to study any part of the upper crust that has been deformed via elasto-frictional mechanisms. Finally, this combined approach may provide more details as to how fold-thrust belts maintain critical-taper and serve as potential targets for natural resource exploration.

Video Link

The video component of this article can be found at <https://www.jove.com/video/54318/>

Introduction

Fold-thrust belts are composed of salients (or segments), where the thrust sheets in adjoining salients are decoupled by recesses or transverse zones^{1,2,3}. The transition from salient to recess may be markedly complex, involving a multifaceted suite of structures, and may hold critical clues to fold-thrust belt development. In this paper, we carefully examine a salient-recess junction, using a combination of multiscale field data and a sandbox model, in order to better understand how deformation can be accommodated within fold-thrust belts.

The junction of the Central Utah segment and the Leamington transverse zone is an ideal natural-laboratory for studying salient-recess junctions for several reasons (**Figure 1**). First, the rocks exposed within the segment continue, uninterrupted, into the transverse zone⁴. So, deformation patterns can be tracked continuously, and compared across the junction. Second, the rocks are essentially monomineralic, so variation in fault patterns are not a result of heterogeneities within units, but instead reflect the overall folding and thrusting within the study area⁴. Third, elasto-frictional mechanisms, such as cataclastic flow, assisted deformation throughout the field area, allowing for direct comparisons of mesoscale fault patterns⁴. Finally, the overall transport direction remained continuous along the length of the segment and transverse zone; therefore, variations in shortening direction did not influence the preserved deformation patterns⁴. All of these factors minimize the number of variables that may have affected the deformation along the segment and transverse zone. As a result, we surmise that the preserved structures formed primarily because of a change in the underlying basement geometry⁵.

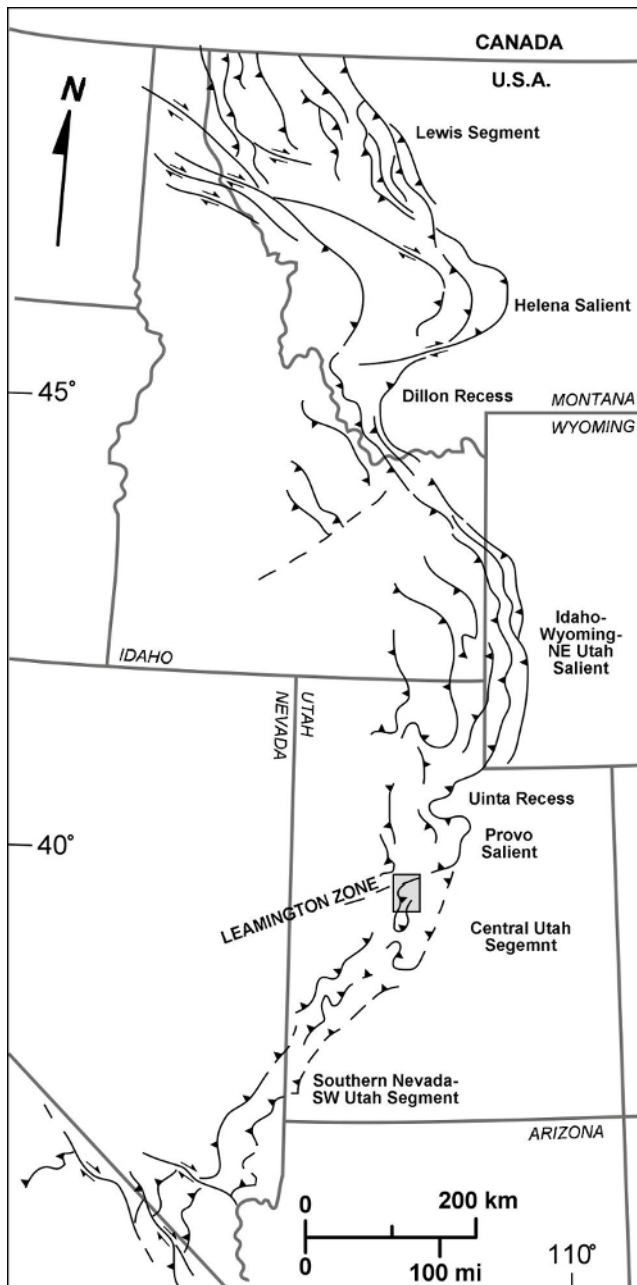


Figure 1. Example of index map. The Sevier fold-thrust belt of western USA, showing major salients, segments, recesses and transverse zones. **Figure 2** indicated by boxed area (modified from Ismat and Toeneboehn⁷). [Please click here to view a larger version of this figure.](#)

Folding and thrusting within the Central Utah segment and Leamington transverse zone, took place at depths < 15 km, *i.e.*, within the elasto-frictional regime, where deformation occurred primarily by outcrop-scale (< 1 m) faults and cataclastic flow^{4,6}. Because transport and folding of the thrust sheet took place primarily by elasto-frictional mechanisms, we predict that a detailed fault analysis can provide further insight into the kinematic history of the Leamington transverse zone and the underlying basement geometry. In order to test this hypothesis, we have collected and analyzed fault patterns preserved in the rocks within the northern portion of the Central Utah segment and throughout the Leamington transverse zone (**Figure 2**).

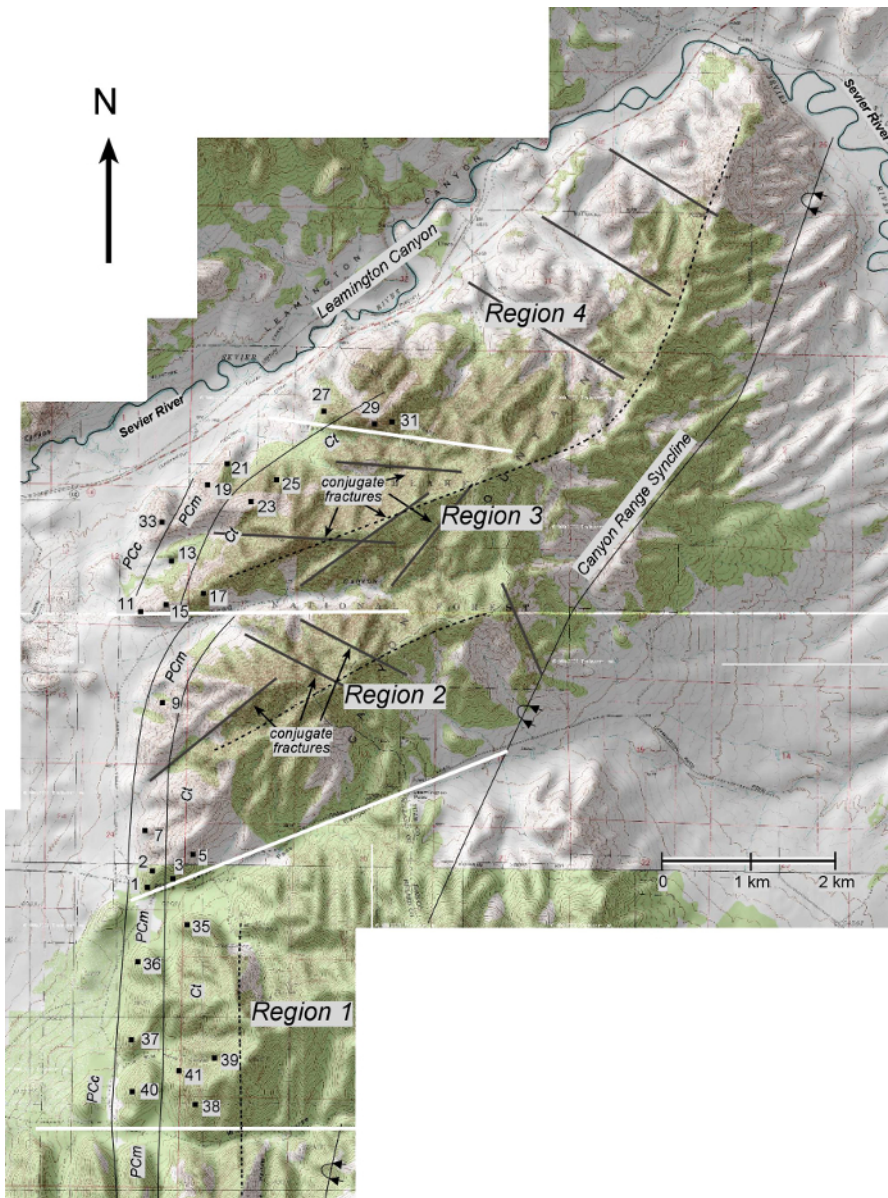


Figure 2. Example of macroscale topographic map. Shaded-relief topographic map of boxed area in **Figure 1**. The 4 Regions are separated by solid white lines. Bedding contacts between the Proterozoic Caddy Canyon quartzite (PCc), Proterozoic Mutual quartzite (PCm) and Cambrian Tintic quartzite (Ct) are shown. Dashed lines show the trend of the mountains within this area. Site locations are shown with numbered black squares. First-order lineations are shown with solid gray lines (modified from Ismat and Toeneboehn⁷). [Please click here to view a larger version of this figure.](#)

Sandbox experiments were carried out to compare against, and supplement, the fault data. A push-block sandbox model, with frontal and oblique ramps, was used to assist our analyses of the structures preserved in, and around, the Leamington transverse zone (**Figure 3**)⁷. The objectives of this approach are four-fold: 1) determine if the mesoscale fault patterns are consistent, 2) determine if the sandbox model supports and explains the field data, 3) determine if the sandbox model provides more details on structures that are not observed in the field, and 4) evaluate whether this combined field-experimental method is useful and easy to replicate.



Figure 3. Example of push-block model. Photograph of empty sandbox model. The southern frontal ramp (SFR), oblique ramp (OR), northern frontal ramp (NFR), and the four Regions (1-4) are labeled (modified from Ismat and Toeneboehn⁷). [Please click here to view a larger version of this figure.](#)

Protocol

1. Collection of Macroscale Field Data

1. Before conducting field work, use aerial photographs/topographic maps to identify the overall trend of the mountains (defined by the modern-day ridge crest), transverse zones, faults and other lineations at the macroscale (**Figure 2**).
 1. Use similar scale topographic maps and aerial photographs, so that patterns can be directly compared. Use 1:24,000 scale maps and photographs.

2. Label and highlight macroscale features on the maps (aerial and/or topographic) to be used in the field. On aerial photographs, use sharp changes in foliage to identify macroscale features, because the foliage patterns reflect the underlying bedrock. On topographic maps, use sharp changes in topography, such as steep cliffs, long narrow valleys and rapid changes in drainage patterns to identify macroscale features.
3. Corroborate these map patterns, with macroscale features found in nature, while in the field. Ensure that the field maps are adjusted accordingly.
4. Subdivide the field area along macroscale transverse zones.

2. Collection of Mesoscale Field Data

1. Conduct field analysis within each transverse zone bound area.
2. Determine the scale of homogeneity of the mesoscale faults throughout the field area. Do this by measuring all faults larger than 3 cm along a transect perpendicular and parallel to the overall macroscale structure. The point at which fault patterns repeat itself along the transect defines the scale of homogeneity.
Note: 3 cm is chosen as a minimum cut-off because faults smaller than 3 cm may be difficult to measure.
3. Choose representative sites throughout the field area using the defined scale of homogeneity.
 1. Ensure that each site contains ~3 mutually perpendicular rock exposures within the scale of homogeneity, in order to quantify the three-dimensional geometry of the fault work.
 2. Ensure that new sites are chosen where the fault patterns markedly change (**Figure 2**).
 3. Choose sites far (~one unit of homogeneity) from major bedding contacts, in order to avoid local shortening and elongation directions that may have overprinted faults produced from the overall shortening direction.
4. Use a grid to keep track of all the faults during data collection⁴.
 1. Ensure that the size of the grid is at the scale of homogeneity of the mesoscale faults. For example, if the faults are homogeneous at the cubic meter scale, use a meter square grid.
5. Construct the grid as a collapsible wooden square — this allows for easier transport in the field.
 1. Use 4 equal pieces of 1 in wide strips of wood. Any type of hard wood is recommended because it is the most durable for field work.
 2. Drill 1/4" holes close to the ends (~ 1/2" from the ends) of the wood strips. Assemble with four 2 1/4" long, 3/16" size screws at each corner. Use steel wing nuts for easiest collapsibility.
 3. Divide the grid equally with string — this helps to track the various faults at each site. Drill holes, equally spaced, along the grids' perimeter, thread and tie string through the holes. For example, for a meter square grid, divide the grid into 10 cm squares with strings connected to the opposite ends of the grid (**Figure 4**).

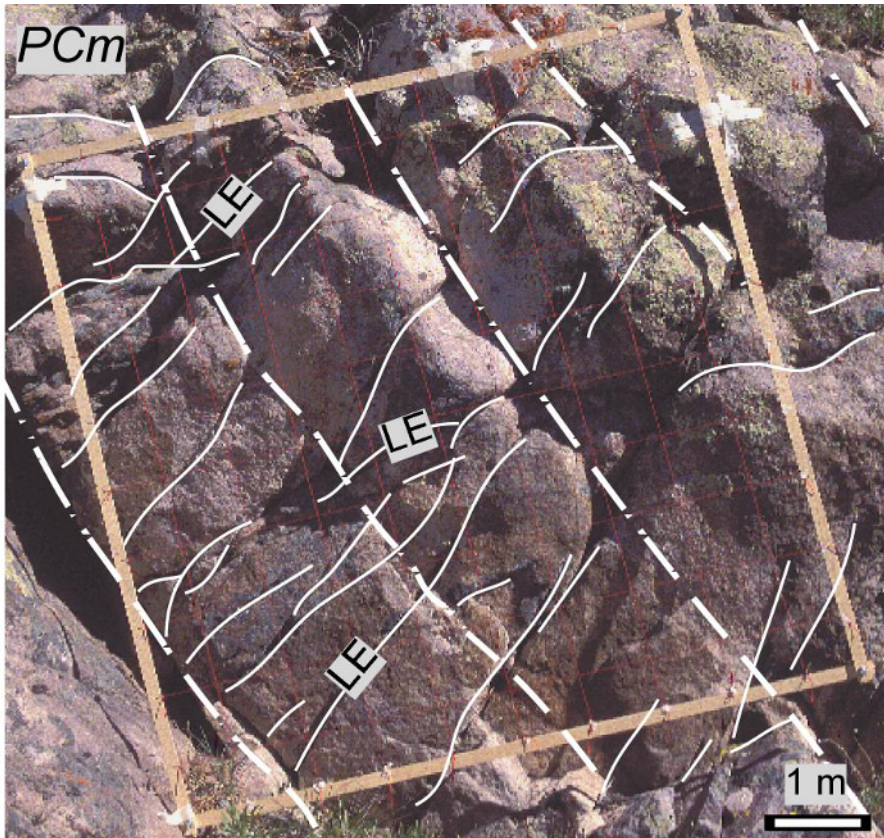


Figure 4. Example of a mesoscale outcrop. Bedding is highlighted with white dashed lines. Specific fault sets discussed in paper are highlighted with thin, solid white lines. m^2 grid is shown (modified from Ismat and Toeneboehn⁷). [Please click here to view a larger version of this figure.](#)

6. Make detailed sketches of the fault sets within each grid.
7. Based on the grid sketches and cross-cutting relationships of the faults, determine the youngest fault sets at each site⁴.
 1. Do this by identifying offset fault patterns at each site. The youngest faults overprint and offset the older faults.
8. At each study site, record the orientation, spacing, length, thickness, and morphological characteristics (e.g., healed, vein filled, open, breccia filled) for each of the youngest faults within each grid.
9. Divide the sites amongst the lithologic units (see **Figure 2**).

3. Collection of Microscale Data

1. Collect oriented rock samples at each site for thin-section analysis.
 1. Ensure that the rock sample is large enough to cut three mutually perpendicular standard size (26 mm x 46 mm) thin-section chips (i.e., slightly larger than an adult fist).
2. Cut thin-section chips (using a standard rock-saw) comparable to the grid orientations from each site, so that the microscale and mesoscale patterns can be directly compared.
3. Prepare standard thickness (0.03 mm) thin-sections⁸.
4. Analyze the thin-sections using a standard optical microscope with an attached camera, for taking photomicrographs.
5. For each thin-section, record morphological characteristics, such as the amount of iron-oxide, and variation and average grain size by using stereological methods, i.e., Spektor Chord analysis (**Table 1**)⁹.
 1. Do this by measuring the width and/or number of chosen morphological characteristics along 4-6 randomly oriented transects through each thin-section^{4,9}. From all of the transects, calculate the average (**Table 1**).

Unit	Bed thickness (m)	Bedding fabric	Grain size (m)	X/Z Fry strain (Average Rf)	X/Y Fry strain (Average Rf)	Amount of overgrowth	Amount of iron oxide	Amount of impurities	Other characteristics
Ct	1,000	Prominent, thick and thin bedded	Ave: 1.59×10^{-4} (Range: 3.6×10^{-6} to 3.31×10^{-4})	1.15	1.12	moderate, semi-connected in small patches	moderate, semi-connected in small patches	moderate, semi-connected calcite in small patches	Ridge former, white to grayish-pink, weathers tan to reddish brown
PCm	570-750	Prominent, well-developed graded and cross-bedding	Ave: 1.48×10^{-4} (Range: 1.15×10^{-4} to 2×10^{-4})	1.22	1.19	major and well-connected	moderate and well-connected	minor calcite and poorly connected	Massive outcrops, purplish red-brown, weathers purple-black

Table 1. Example of microscale morphology. Description of the Proterozoic Mutual (PCm) and Eocambrian Tintic (Ct) quartzite units. X/Z Fry strain is measured in a vertical section parallel to the transport plane, while X/Y Fry strain is measured in a vertical section perpendicular to the transport plane (modified from Ismat and Toeneboehn⁷). [Please click here to view/download this table in Microsoft Excel format.](#)

- Measure strain using normalized Fry analysis^{10,11}. Ensure that strain is measured from three mutually perpendicular thin-sections in order to determine three-dimensional strain at each site.
 - Do this by taking a photomicrograph of each thin-section. Ensure that the photomicrographs contain at least 50 grains with solid grain boundaries, *i.e.*, not sub-grain boundaries.
 - Define the outlines of the grains in order to measure Fry strain. Define the outlines either manually, by tracing the outlines from a printed photomicrograph onto tracing paper, or digitally, by uploading the photomicrograph into an image analysis software program (*e.g.*, Image Pro Plus) that automatically defines the grains' boundaries.
 - Upload the grain boundary image into the normalized Fry Strain program¹².

4. Plotting Mesoscale Fault Data

- Analyze the fault data on Equal-area nets. For example, use *Stereonet* (freeware from R.W. Allmendinger).
 - Plot the fault sets' poles on Equal-area nets and then contour these poles using 1% area contours (**Figure 5**).
 - Determine the most common fault sets from these pole concentrations. Plot these fault sets as great-circles (**Figure 5**).

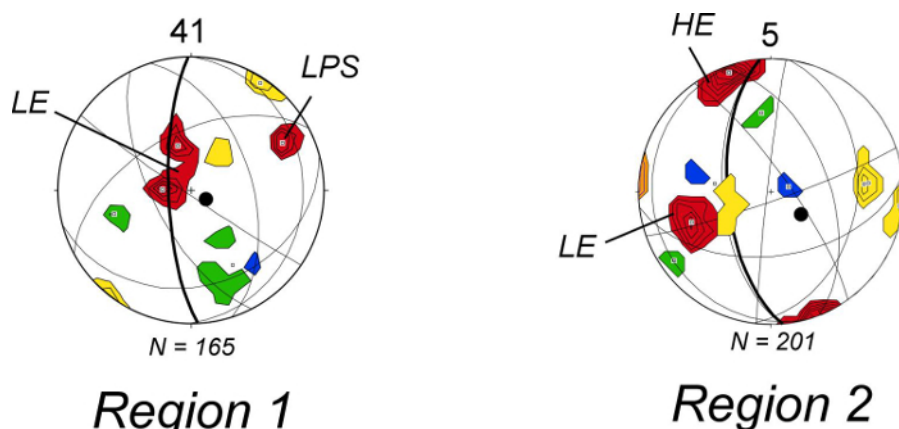


Figure 5. Examples of Equal-area plots. Equal-area plots of fault sets from two sites — site 41 is from Region 2 and site 5 is from Region 1. Fault sets are plotted as contoured poles (1% area contours). Average fault sets are determined from pole-concentrations and plotted as great circles. Maximum shortening directions, determined from conjugate-conjugate fault sets, are plotted as black dots. Fault-pole contours are colored according to percentage contribution at each site. Pole concentrations that contribute to >20% are colored red, between 15-19% are colored orange, 10-14% are yellow, 5-9% are green and <5% are colored blue. Red fault-pole contours are labeled as LPS (layer-parallel shortening), LE (limb extension), and HE (hinge-extension) (modified from Ismat and Toeneboehn⁷). [Please click here to view a larger version of this figure.](#)

- Identify the conjugate fault sets, *i.e.*, the great-circle pairs with dihedral angles that range from 40° to 75° (**Figure 5**)¹³.
- Define the acute bisector of the conjugate-conjugate fault sets — this locates the maximum shortening direction (**Figure 5**)^{4,14,15}.
- Further subdivide the equal-area net fault-pole concentrations, according to their percentage contribution for each site. Do this by color coding the pole concentrations, for easier visual analysis. For example, highlight pole concentrations that contribute to >20% of the overall poles for that site red. Color those that contribute between 15-19% orange, 10-14% yellow, 5-9% green and <5% blue (**Figure 5, Table 2**).

Site	Bedding	Shortening	Highest fault-pole	Fault sets(s)
	(dip, dip direction)	direction(s)	concentration(s)	(dip, dip direction)
		(plunge, trend)	(plunge, trend)	
41	83, 268	79, 115	22, 064	68, 244
			60, 345	30, 265
			73, 276	17, 096
5	63, 265	67, 130	08, 343	82, 263
			36, 247	54, 067

Table 2. Example of mesoscale fault data. Chart, showing just 2 of the 24 sites, documenting the following: bedding orientation, shortening direction(s), orientation of the highest fault pole concentration(s) and their corresponding fault set(s) (modified from Ismat and Toeneboehn⁷).

- Label the pole concentrations according to different fault types (e.g., hinge extension) (**Figure 5**).
- Label the different fault types on the mesoscale photos, for easier visual analysis (**Figure 4**).
- Graph the different fault types, for easier visual analysis (**Figure 6**). Do this by graphing the fault data along and across the overall macroscale structure.

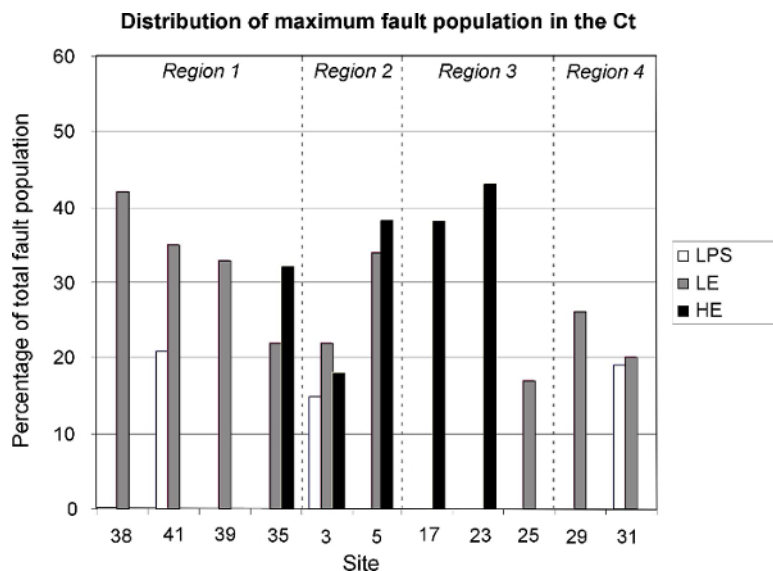


Figure 6. Example graph showing distribution of fault populations. Graph showing the percentage and type of the maximum fault sets (highlighted in red in **Figure 5**) for each site. Just sites within the Ct quartzite are shown here (modified from Ismat and Toeneboehn⁷). [Please click here to view a larger version of this figure.](#)

5. Construction of the Push-block Sandbox Model

- Use $\frac{3}{4}$ inch MDF (medium-density fiberboard) to reduce potential surface heterogeneities arising from wood grain, coarsely planed surfaces, or other defects from lumber (**Figure 3**).
- Apply a basic finishing lacquer to seal the surfaces of the MDF board and prevent epoxy (described below) from permeating the model's surfaces (**Figure 3**).
- Scale and orient the sandbox model to the field area. For example, in this study, model the length of the box to represent the EW trend line, and model the width of the box to represent the NS trend line. Scale the sandbox model where 4 cm is equal to 1 km (**Figure 3**).
- Construct the box larger than the field study area in order to avoid potential boundary conditions and/or edge effects from the model.
 - Do not construct a backstop, in order to allow sand to pass without an unrealistic boundary (**Figure 3**).
- Build a push-block equivalent to the width of the sandbox. This will prevent sand from passing through the sides of the push-block.
 - Use $\frac{3}{4}$ inch MDF for the push block.
- Attach the push-block to a crank driven threaded metal bar (**Figure 7**).
 - Use a 4-6 inch diameter circular crank with a handle — a circular crank puts less strain on the attendant's wrist and hands.
 - Use a zinc-plated threaded bar (preferably acme threaded) that is at least $\frac{3}{4}$ inch in diameter. If the bar is too thin, it may not be able to withstand the weight of the sand.
 - Ensure that the length of the threaded bar extends from the beginning of the sandbox to the end of the ramps.

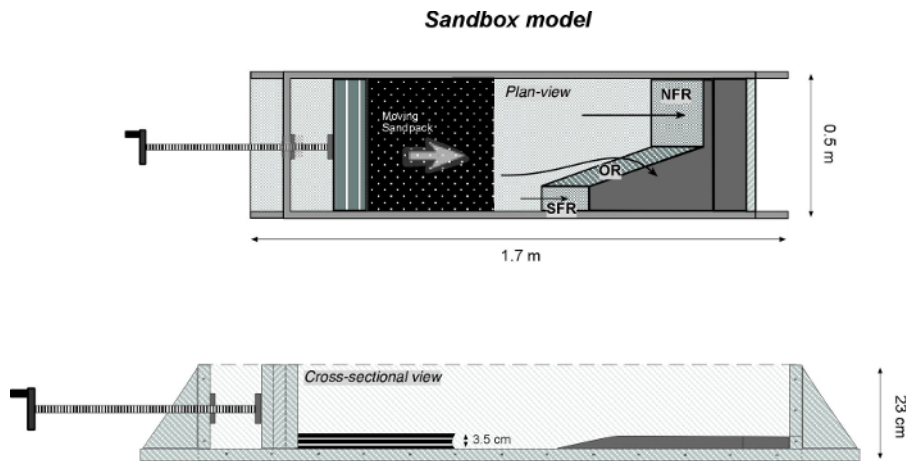


Figure 7. Example sandbox model diagram. Diagrams for the sandbox model, illustrated as plan and cross-sectional views. The southern frontal ramp (SFR), oblique ramp (OR) and northern frontal ramp (NFR) are labeled. Thin arrows drawn over the ramps illustrate potential direction of sand movement. See **Figure 3** for a photograph of an empty sandbox model (modified from Ismat and Toeneboehn⁷). [Please click here to view a larger version of this figure.](#)

7. Drill an elongated hole, with a vertical long axis, in the center of the frontstop. This elongated shape will allow the push-block (attached to the threaded bar) to move up and over the ramps, if needed (**Figure 8**).
 1. Ensure that the length of the elongated hole is equal to the height of the tallest ramp.
 2. Secure the elongated hole with a metal frame. Attach the metal frame to the frontstop with nuts and bolts (**Figure 8**).
 3. Thread the rod through a matching pitch and diameter nut mounted to the frontstop (**Figure 8**).

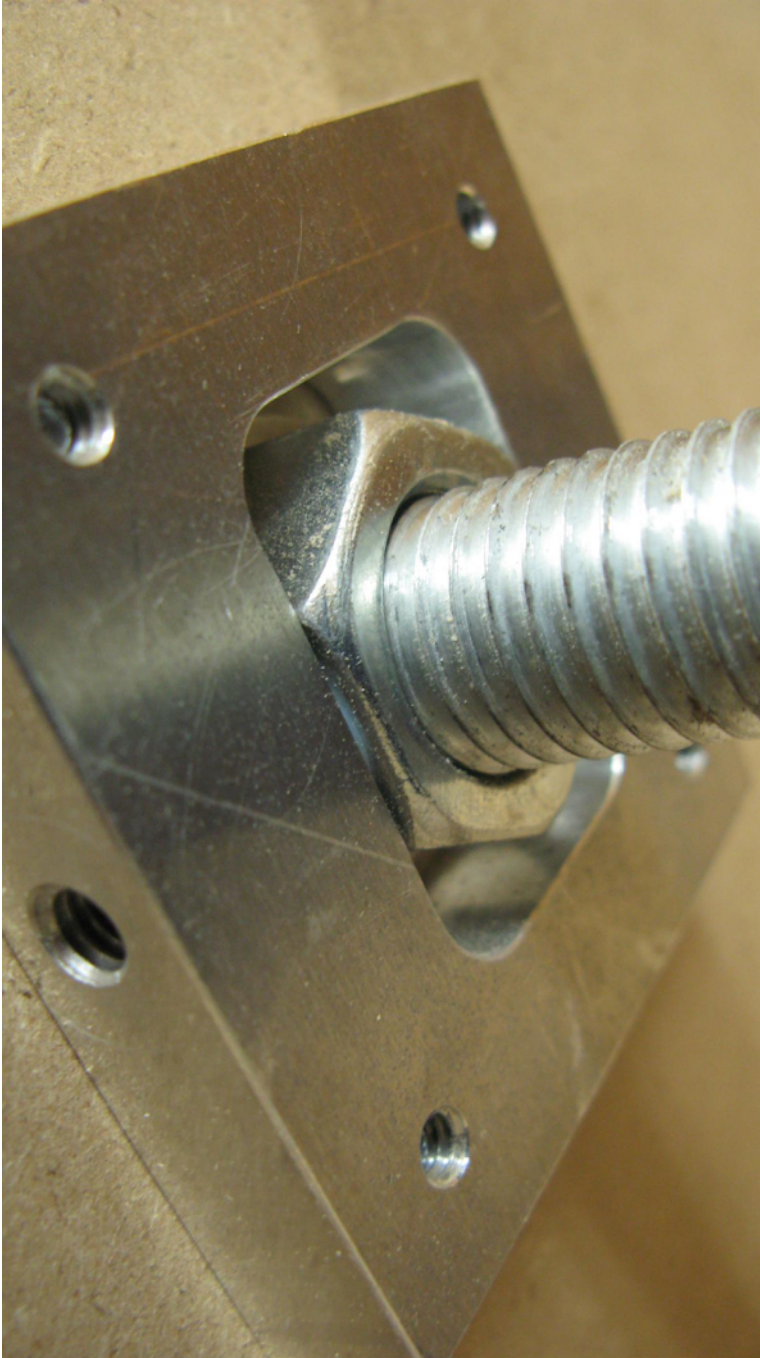


Figure 8. Example threaded bar connection. Close-up view of the threaded bar and matching nut mounted to the frontstop. [Please click here to view a larger version of this figure.](#)

8. Construct an oblique ramp, bound on both sides by frontal ramps. Construct the ramps out of pine with glued rabbet joints on the top surfaces and countersunk fasteners along the base.
 1. Cut the ramps at comparable orientations to what is predicted in the field.
 2. Expand the distance between the various ramps, as compared to what is observed in the field, so that the structures that form in the sand are more visible.
9. Sand the surfaces with a fine grit sanding paper to remove surface heterogeneities and apply a polyurethane finish to protect the soft wood.
10. Cover the ramps and the base of the sandbox with painters tape to protect the wood from epoxy between trials. Ensure that the tape is smooth and free from ridges or flaps.

6. Running the Push-block Sandbox Model

1. Use typical play-sand. This type of sand is relatively homogeneous, with an average grain size of 0.5 mm.

2. Dye and dry half of the sand.
 1. Fill a 5-gallon bucket a quarter full with play-sand and add black food coloring while mixing until a uniform dark green color is attained. Use as much dye as is needed to make the color of the dyed sand clearly distinctive from the undyed sand.
 2. Allow sand to dry at room temperature, which may take several days, or in an oven (up to 500 °C), which may only take a few hours. Do not place hot sand in the sandbox. Ensure that the sand has cooled to room temperature before use.
3. Lay the sand in alternating layers of colored and uncolored (tan) sand. Test various thicknesses of sandpacks. In this set-up, the clearest and most reproducible results were produced with a sandpack 3.5 cm thick, with alternating colored and tan layers 0.6 cm thick (**Figure 7**).
4. Gently press a plastic mesh, composed of 0.5 in² (1.3 cm²) squares onto the top of the undeformed sand to produce a grid indentation (**Figure 9**).

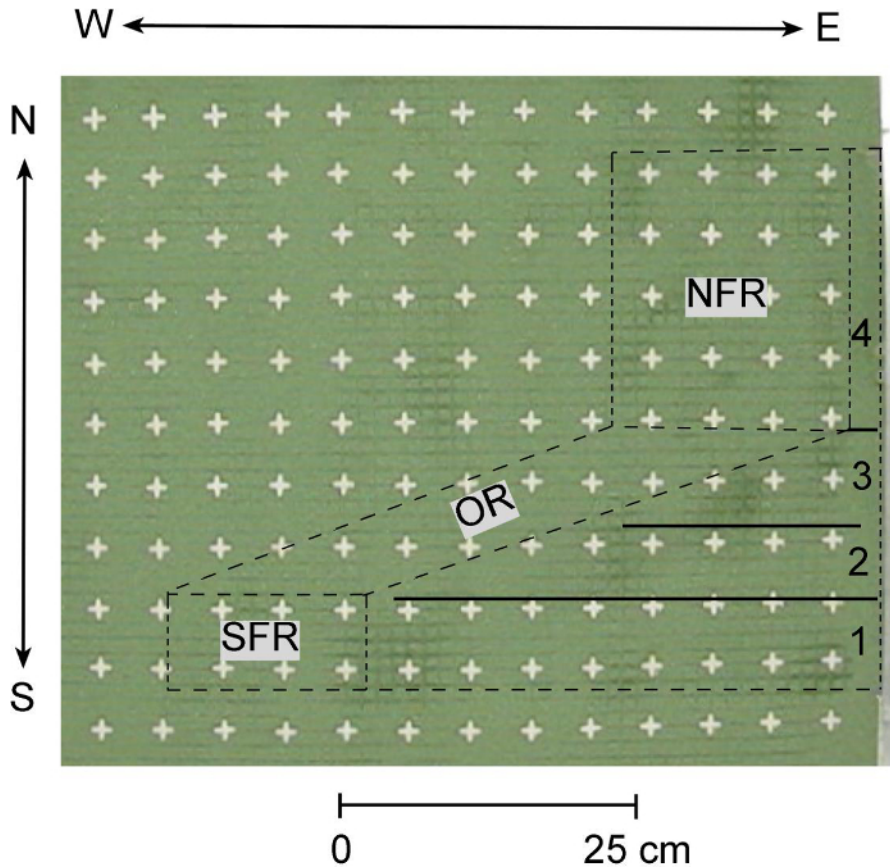


Figure 9. Example of undeformed sand in sandbox model. Partial plan-view of undeformed sand in sandbox model. Note grid indentation and square cross-pins. The southern frontal ramp (SFR), oblique ramp (OR), northern frontal ramp (NFR), and the four Regions (1-4) are labeled (modified from Ismat and Toeneboehn⁷). [Please click here to view a larger version of this figure.](#)

5. Insert square cross pins 2 inches (~5 cm) apart throughout the undeformed sand (**Figure 9**).
6. Push the sand with the crank driven push-block. In this set-up, move the sand 60 cm, *i.e.*, 60 cm of shortening (**Figure 10**).
 1. Move the push-block slow enough so that changes in the sand can be carefully documented. The speed at which the push-block is moved (*i.e.*, strain rate) does not affect the results.
 2. Track the deformation by observing the shape changes of the squares (**Figure 10**).
 3. Track the amount of transport and vertical rotation by observing the motion of the pins (**Figure 10**).
 4. Document all of these changes with a camera mounted near the sandbox, so that the entire sandbox is within the picture field. Ensure to take still frame photographs as well as videos.

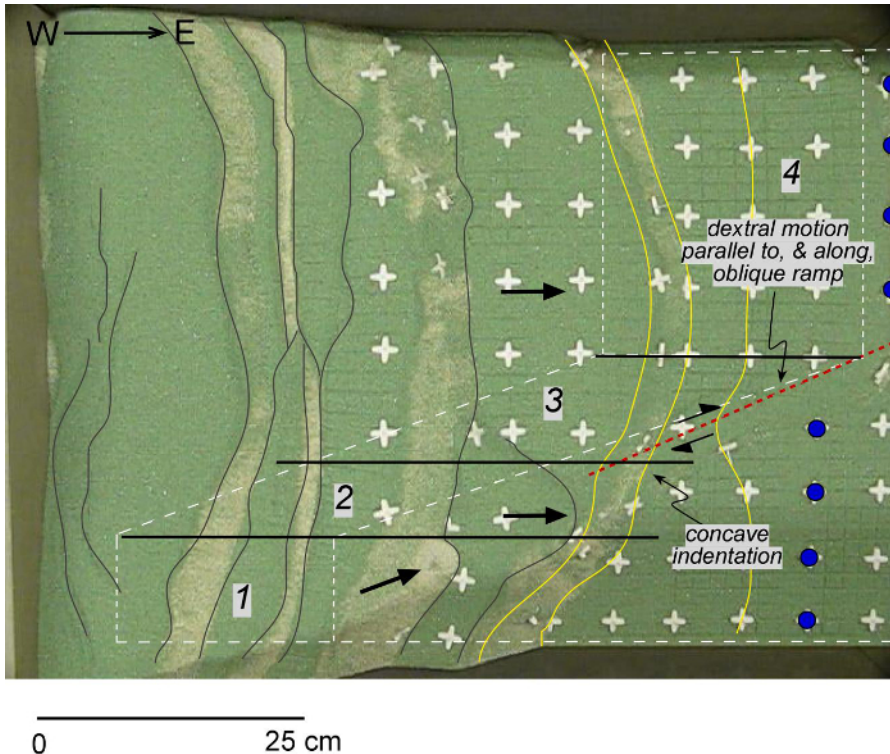


Figure 10. Example of deformed sand layers. Plan-view of the end-result deformation from the sandbox model. Select cross-pins labeled with blue dots showing dextral offset. Folded cross-pins highlighted with yellow lines. Thrust faults are highlighted with thin, black lines. The four Regions (1-4) are labeled (modified from Ismat and Toeneboehn⁷). [Please click here to view a larger version of this figure.](#)

7. Experiment with varying amounts of sand and total shortening.
 1. Repeat until satisfied, *i.e.*, until the structures formed in the sandbox mimic those preserved in nature, under comparable shortening amounts.

7. Collecting Samples from the Sandbox

1. Remove all cross-pins from the sand once the sandbox results mimic those preserved in nature.
2. Collect samples from the sandbox by separating and epoxying portions of the deformed sand (**Figure 11**).
 1. Do this by constructing two pre-cut sheet-metal dividers to isolate portions of the deformed sand (**Figure 9**).
 2. Ensure that the bottom edge of the divider is cut to match the angle of the ramp.
 3. To protect the dividers from epoxy between trials, cover the dividers with painters tape (**Figure 11**).
 4. Ensure that the dividers extend over and beyond the ramps. In this study, use rectangular dividers that measured 45 cm long and 9 cm wide (**Figure 11**).
 5. Ensure that the dividers are taller than the thickest portion of the deformed sandpack (**Figure 11**).
 6. Ensure that one end of the divider is closed, in order to control the flow of the epoxy. Do not close the other end of the divider, in order to minimize any potential disturbance to the sandpack (**Figure 11**).

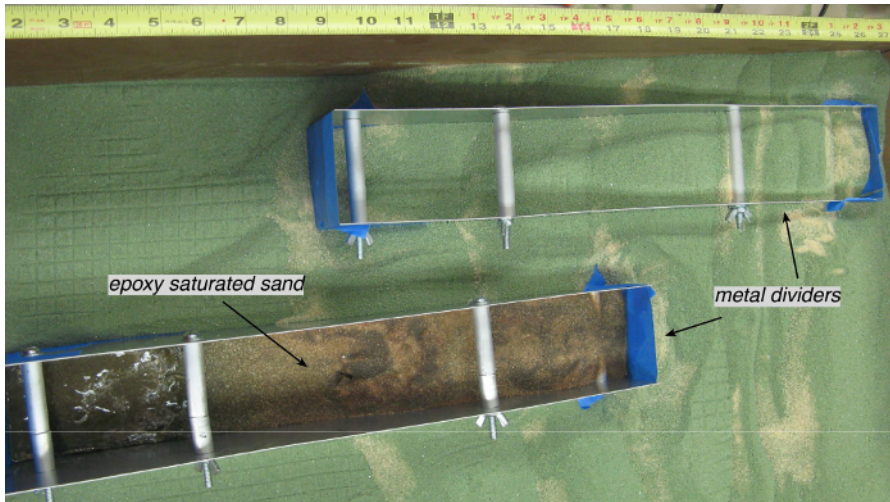
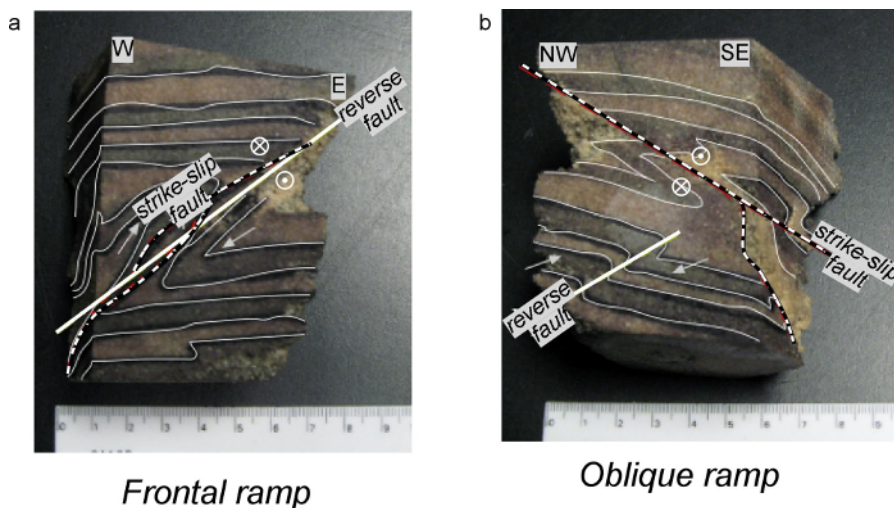


Figure 11. Example of metal dividers. Plan-view, showing 2 metal dividers, one through a frontal ramp and one through the oblique ramp, in the deformed sand. The metal divider along the oblique ramp is filled with epoxy. Note tape measure for scale (Modified from Ismat and Toeneboehn⁷). [Please click here to view a larger version of this figure.](#)

3. Steady the dividers with metal bars (**Figure 11**).
 1. Do this by fastening the dividers with $\frac{1}{4}$ inch x 4 inch machine screws through pre-drilled holes toward the top of the dividers. Sheath the screws with $\frac{3}{8}$ inch diameter aluminum tubing between the divider's sides. In this study, use two metal bars for each divider (**Figure 11**).
4. Place one divider on the oblique ramp, and the second on the frontal-oblique ramp junction (**Figure 11**).
5. Pour warmed epoxy across the top of the sand portions isolated by the metal dividers (**Figure 11**).
 1. Continue to pour epoxy until it is no longer absorbed by the sand. This ensures that the sand is fully saturated.
6. Pull the epoxied areas out of the metal dividers, once the epoxy is dry. Do this by pulling the dividers out with the metal bars.
7. Using a rock saw, cut the epoxied areas perpendicular and parallel to the strike of the ramps.
8. Highlight the bedding, folds and faults with a permanent marker on the epoxied samples (**Figure 12**).



Frontal ramp

Oblique ramp

Figure 12. Examples epoxied samples from sandbox model. Epoxied samples from the (a) northern frontal ramp and the (b) oblique ramp within the sandbox model. Shown samples are cut perpendicular to the trend of the ramps. Layers are highlighted with thin, white lines. Solid white lines mark reverse faults, dashed white lines mark strike-slip faults (modified from Ismat and Toeneboehn⁷). [Please click here to view a larger version of this figure.](#)

9. Compare the sandbox samples to the field data.
 1. Compare samples with cross-sections from the area. Be sure the samples and cross-sections have similar orientations.

Representative Results

Aerial photographs were used to subdivide the field area into four Regions (1–4), based on the trend of the modern mountain ridge crest (**Figure 2**). Multi-scale fault data is compared between these four Regions. Assuming that these trend changes reflect the underlying basement geometry, the oblique ramp is positioned within Regions 2 and 3, where the mountains trend oblique to the Sevier fold-thrust belt. Throughout the four Regions, we found that the mesoscale faults preserve a deformation fabric that is penetrative and homogeneous at the mesoscale (*i.e.*, cubic meter of rock) and are representative of areas larger than the cubic meter sites (**Figure 4**)^{4,16}. In addition, microscale variations, shown in **Table 1**, are not reflected in the collective character of fault patterns. So, the mesoscale fault sets can be directly compared throughout all four Regions (**Figure 5**). In brief, we found that the mesoscale faults sets can be defined as conjugate-conjugate sets and rotate with bedding, which entail that the shortening directions do, too. This pattern suggests that the mesoscale faults formed early, and different combinations of fault sets are used to assist the fold shape. In more detail, we found that the fault patterns are unique within each of the four regions — Regions 2 and 3, and Regions 1 and 4, are similar to each other (**Figure 6**). This pattern supports the macroscale assumption that the oblique ramp underlies Regions 2 and 3, and suggests that our conjugate-conjugate fault analysis is reliable. Beyond that, however, this method of analysis is not any more illuminating. Because of this, we further analyzed the fault data by examining the Equal-area net fault-pole concentrations (**Figure 5**). This approach is used to track which of the youngest sets were most dominant during deformation. These patterns also suggest an oblique ramp underlying Regions 2 and 3, and unlike the conjugate-conjugate fault analysis, reveal a sharp break between these two Regions. Therefore, we interpret that this pole-concentration analysis is reliable and potentially elucidates subtle structures that may not be clear from the conjugate-conjugate fault method.

Similar to previous models, based on finite element modeling (FEM) we have assumed that the oblique ramp is continuous¹⁷. The sharp break in bedding and fault patterns across the boundary between Regions 2 and 3 can be explained by differential motion over a continuous oblique ramp. Alternatively, the discontinuity in bedding and fault patterns across Regions 2 and 3 may reflect a break in the underlying basement. Here, we compare our field data to our sandbox model results in order to test these two hypotheses. We found that a break in the overlying thrust sheet formed even though there was no break in the basement (**Figure 10**). Interestingly, the location and orientation of the break is comparable to the position and orientation of the boundary between Regions 2 and 3 on the macroscale maps. Therefore, the break observed in the overlying thrust sheet may have simply formed via a complex interaction of an eastward moving thrust sheet over an oblique ramp. In other words, deformation preserved in thrust sheets may not directly mirror the underlying basement geometry. So, this sandbox experiment successfully replicates, and potentially explains, fault patterns preserved in the field.

The epoxied sandbox samples were analyzed from the sandbox model to observe the internal structure of the deformed sand, and compare these structures against field observations. Two representative samples were analyzed — a sample from the frontal and oblique ramps (**Figure 12**). In general, the reverse faults and folds preserved in the epoxied samples from the frontal ramp accommodate transport to east, and those from the oblique ramp accommodate transport to the southeast. The strike-slip faults in all the samples accommodate dextral motion. This kinematic record along the frontal and oblique ramps supports previous models^{17–19}, as well as the mesoscale fault data. These hand samples are novel way to analyze internal structures that may not be accessible in the field.

Discussion

The Central Utah segment of the Sevier fold-thrust belt, and its northern boundary, the Leamington transverse zone serves as an ideal natural laboratory for studying salient-recess junctions (**Figure 1**). Along this junction, the transport direction remains constant and the thrust sheets are uninterrupted across the junction, so the only variable is the underlying basement geometry⁵.

Here, we present a method to analyze this type of salient-recess junction by combining multi-scale fault data collected in the field with a push-block sandbox model, which replicates the large-scale geometry of the field area. The sandbox model experiment represents a longer time period of deformation than the mesoscale fault sets — we assume that the youngest fault sets accommodated the observed fold geometry. So, the sandbox model, in conjunction with the faults sets, can be used to track thrust sheet deformation and determine details of the underlying basement geometry.

In order for this combined approach to be successful, the following critical steps need to be taken in the field and sandbox experiment. For the field portion, it is critical to determine the scale of fault homogeneity — fault sets that are not preserved at equivalent scales cannot be directly compared. In addition, a large population of faults (≥ 30 fault sets) need to be measured in order ensure statistically reliable data sets⁹. Moreover, faults should be measured away from heterogeneities, such as bedding contacts, in order to avoid local strain variations. Even microscale variations, such as impurities, a range in grain size and large amount of strain ($F_y > 1.8$) may influence mesoscale fracture development by creating foliation planes and other heterogeneities. For the experimental portion, the sandbox model must mimic the field geometry as closely as possible. It is recommended that the box be constructed at a larger scope than the field area, in order to avoid edge-effect complications. The macroscale Regions were also enlarged, for the same reason. It is important that the grain size of the sand mimics Coulomb behavior²⁰ — an average grain size of ~ 0.5 mm is recommended²¹. Finally, once the experiment is being run, it is critical that the large scale faults and folds form in the same orientations and order (*e.g.*, forward breaking, backward breaking, *etc.*) as observed in the field. Otherwise, the structures formed in the model cannot be compared to the field data, even if they look similar.

The results from this study are comparable to, and support, previous work conducted in this area based on FEM^{17,22}, and provides more details to the kinematic history. This suggests that detailed fault data, measured in areas that have deformed by elasto-frictional mechanisms, can be used to develop more detailed kinematic models than some computer models. Although fault data collection and analyses is laborious and time consuming, this method may be more accessible than computer and analog modeling, and is less expensive. Fractures and faults are often overlooked²³ — many geologists view upper crustal deformation as minor and void of patterns. However, a large portion of the crust — the upper ~ 15 km — deforms by faulting and other elasto-frictional mechanisms. This work suggests that a significant amount of geologic history is stored in the upper crust and is readily available for analysis.

We demonstrate that even in the simplest cases, such as examined here, the structures preserved in the upper crust do not necessarily mimic the underlying basement geometry. Detailed fault analyses can reveal subtleties that may not be revealed with map patterns, standard conjugate fault studies and/or computer models, such as FEM. Using a sandbox model can help explain why some of these subtle patterns exist. This method presented here is simple, reliable and easy to replicate. It can potentially change how many geologists perceive the role of faults and cataclastic flow, and what they can tell us. This method can be used to re-examine, and uncover more kinematic details, of underexplored field areas, and can be easily modified to accommodate geologic settings other than fold-thrust belts. This approach has far reaching implications in terms of tracking fracture controlled fluid flow in the upper crust as well as how fold-thrust belts maintain critical taper at salient-recess junctions.

The main weakness of this approach is that sandbox modeling may not be able to replicate complex geologic histories. For example, in cases where there are variable shortening directions, the timing and direction of events should be carefully tracked in the field and then replicated with different push-blocks in the sandbox model. However, the sand will likely not preserve these various directions of shortening because the sand will flow and bedding layers will not be maintained. This problem may be resolved by adding oil or petroleum jelly to the sand, to make the sand more cohesive. But, then the sand will not behave as a Coulomb material and thus, may not model deformation in the upper crust. Further work is required to unravel more complex natural systems, such as situations where the basement geometry not the only variable.

Disclosures

The authors have nothing to disclose.

Acknowledgements

We thank Erin Bradley and Liz Cole for their assistance in the field. Field work, thin-section preparation and material for the sandbox model was supported by Franklin & Marshall College's Committee on Grants.

References

1. Marshak, S., Wilkerson, M.S., & Hsui, H.T. Generation of curved fold-thrust belts: Insights from simple physical and analytical models, In: *Thrust Tectonics*. McClay, K.R., ed., Chapman and Hall, 83-92 (1992).
2. Mitra, G. Evolution of salients in a fold-and-thrust belt: the effects of sedimentary basin geometry, strain distribution and critical taper. In: *Evolution of Geological Structures in Micro- to Macro-scales*. Sengupta, S., ed., Chapman and Hall, 59-90 (1997).
3. Weil, A., & Sussman, A. Classifying curved orogens based on timing relationships between structural development and vertical axis rotations. In: *Orogenic curvature Geol. Soc. of Am. Special Paper*. Volume 383, Sussman, A., Weil, A., eds., 205-223 (2004).
4. Ismat, Z., & Mitra, G. Folding by cataclastic flow at shallow crustal levels in the Canyon Range, Sevier orogenic belt, west-Central Utah. *J. of Struct. Geol.* **23** (2-3), 355-378 (2001).
5. Tull, J., & Holm, C. Structural evolution of a major Appalachian salient-recess junction: Consequences of oblique collisional convergence across a continental margin transform fault. *Geol. Soc. of Am. Bull.* **117** (3), 482-499 (2005).
6. Ismat, Z., Block supported cataclastic flow within the upper crust. *J. of Struct. Geol.* **56**, 118-128 (2013).
7. Ismat, Z., & Toeneboehn, K. Deformation along a salient-transverse zone junction: An example from the Leamington transverse zone, Utah, Sevier fold-thrust belt (USA). *J. of Struct. Geol.* **75**, 60-79 (2015).
8. Reed, F.S., & Mergner, J.L. Preparation of Rock Thin Sections. *Amer. Mineral.* **38**, 1184-203 (1953).
9. Underwood, E.E. *Quantitative Stereology*. Addison-Wesley Publishing Company (1970).
10. Fry, N. Random point distribution and strain measurement in rock. *Tectonophysics*. **60** (1), 89-105. point distribution and strain measurement in rock (1979).
11. McNaught, M.A., Estimating uncertainty in normalized Fry plots using a bootstrap approach. *J. of Struct. Geol.* **24**(2), 311-322 (2002).
12. De Paor, D. G., An Interactive Program for Doing Fry Strain Analysis on the Macintosh Microcomputer. *J. of Geol. Ed.* **37**(3), 171-180 (1989).
13. Ismat, Z. Folding kinematics expressed in fracture patterns: An example from the Anti-Atlas fold-belt, Morocco. *J. of Struct. Geol.* **30** (11), 1396-1404 (2008).
14. Reches, Z., Faulting of rocks in three-dimensional strain fields: II. Theoretical analysis. *Tectonophysics*. **95**(1-2) 10.1016/0040-1951(83)90264-0 (1983).
15. Reches, Z., & Dieterich, J. H. Faulting of rocks in three dimensional strain fields: 1. Failure of rocks in polyaxial, servo-control experiments. *Tectonophysics*. **95** (1-2), 111-132 1 (1983).
16. Ismat, Z. Evolution of fracture porosity and permeability during folding by cataclastic flow: Implications for syntectonic fluid flow. *Rocky Mount. Geol.* **47** (2), 133-155 (2012).
17. Kwon, S., & Mitra, G. Three-dimensional kinematic history at an oblique ramp, Leamington zone, Sevier belt, Utah. *J. of Struct. Geol.* **28** (3), 474-493 (2006).
18. Casas, A.M., Simon, J.L., & Seron, F.J. Stress deflection in a tectonic compressional field: A model for the northeastern Iberian chain, Spain. *J. of Geophys. Res.* **97**, 7183-7192 (1992).
19. Apotria, T.G. Thrust sheet rotation and out-of-plane strains associated with oblique ramps: An example. *J. of Struct. Geol.* **17** (5), 647-662 (1995).
20. Hubbert, M.K. Theory of Scale Models as Applied to the Study of Geological Structures. *Geol. Soc. of Am. Bull.* **48** (10), 1459-1520 (1937).
21. Schöpfen, M.P.J., & Steyrer, H.P. Experimental modeling of strike-slip faults and the self-similar behavior. In: *Tectonic Modeling: A volume in honor of Hans Ramberg Geol. Soc. of Am. Mem.* Volume 193, Koyi, H.A., Mancktelow, N., eds., 21-27 (2001).
22. Kwon, S., & Mitra, G. 2004. Strain distribution, strain history and kinematic evolution associated with the formation of arcuate salients in fold-thrust belts: the example of the Provo salient, Sevier orogeny, Utah. In: *Orogenic curvature Geol. Soc. of Am. Special Paper*. Volume 383, Sussman, A., Weil, A., eds., 205-223 (2004).
23. Elliott, D. The motion of thrust sheets. *J. of Geophys. Res.* **81**, 949-963 (1976).